



Geophysical Research Letters

Supporting Information for

Widespread Aseismic Slip Along the Makran Megathrust Triggered by the 2013 Mw 7.7 Balochistan Earthquake

Xiaoran Lv^{1,2}, Falk Amelung³, and Yun Shao^{1,2,4*}

¹ Aerospace Information Research Institute, Chinese Academy of Sciences, Beijing 100094, China.

² University of Chinese Academy of Sciences, Beijing 100049, China.

³ Rosenstiel School of Marine and Atmospheric Sciences, University of Miami, Miami, FL 33149, USA.

⁴ Laboratory of Target Microwave Properties (LAMP), Zhongke Academy of Satellite Application in Deqing (DASA), Deqing 313200, China. [Institutional affiliations]

Contents of this file

Text S1 to S8

Figures S1.1 to S7.4

Tables S1 to S4

Additional Supporting Information (Files uploaded separately)

Table S2.1. Range, optimal and uncertainties of InSAR-inversion fault slip parameters of the down-dip extension model for time period 1.

Table S2.2. Same as Table S2.1 but for the secondary fault model of time period 1.

Table S2.3. Same as Table S2.1 but for basal decollement model of time period 1.

Table S2.4. Same as Table S2.1 but for mid-prism decollement model of time period 1.

Table S3.1. Same as Table S2.1 but for time period 2

Table S3.2. Same as Table S2.3 but for time period 2.

Table S3.3. Same as Table S2.4 but for time period 2.

Table S4. Direction (rake) of maximum coseismic shear stress and aseismic slip of basal decollement model and mid-prism decollement model.

Introduction

This supplement contains 8 sections. First we demonstrate that the tropospheric delays are successfully corrected using the ERA5 weather model (section S1). Next we discuss whether the InSAR data could contain linear ramps that are not taken into account in our modelling approach (section S2). We then discuss two additional viscoelastic models to potentially explain the post-seismic observations, a linear Maxwell and power law model with $n=2$ (section S3.1). In the same section we also present a model for the simulated surface LOS deformation caused by the viscoelastic relaxation occurring at 40-50 km depth (section S3.1) and we compare our cumulative displacements with the results of Peterson et al. (2018) (section S3.2). We then present for our four aseismic slip models, the observation-model fit and observation-residual results in original quadtree downsampled format, for time period 1 (section S4) and time period 2 (section S5), respectively. In the following section we present a strength profile (Section S6) for the Makran accretionary prism. Finally, we discuss the coulomb stress change (Section S7) on the best-fitting aseismic slip models imparted by the coseismic fault with effective friction coefficient of 0 and 0.7 and compare the direction of maximum coseismic shear stress and the direction of aseismic slip along the decollement faults.

S1. Validation of the tropospheric delay correction

The stratified tropospheric delay is not random in time but seasonal, and varies with surface elevation which means its spatial pattern always mimics elevation (Doin et al., 2009). If there is a significant elevation difference between two locations, the stratified tropospheric delay varies with the seasons. Therefore, the InSAR LOS time series (after correcting the topography error and solid earth tide phase) between these two locations can be dominated by the seasonal variations of tropospheric delay (Jolivet et al., 2011; Jolivet et al., 2014; Fattah and Amelung, 2015). In this section, we investigate whether this phenomenon is reflected in our InSAR data and explore whether the ERA5 model describes the tropospheric delay well.

The Hoshab fault is located ~100 km from the Makran coast at 0.9 km elevation (Figure S1.1b). To investigate whether the ERA5 weather model properly describes tropospheric delays related to this elevation difference, we consider the difference between a pixel located at the Hoshab fault and a reference pixel located at the south end of the profile (elevation difference of 970 m over a horizontal distance of about 88 km; yellow squares in Figure S1.1a). The InSAR range change (after correcting the solid earth tide effects and topographic residuals) and the relative tropospheric delay time series calculated using ERA5 data (Figure S1.2) have the same temporal trends, which indicates that the ERA5 weather model describes the tropospheric delay well in this area.

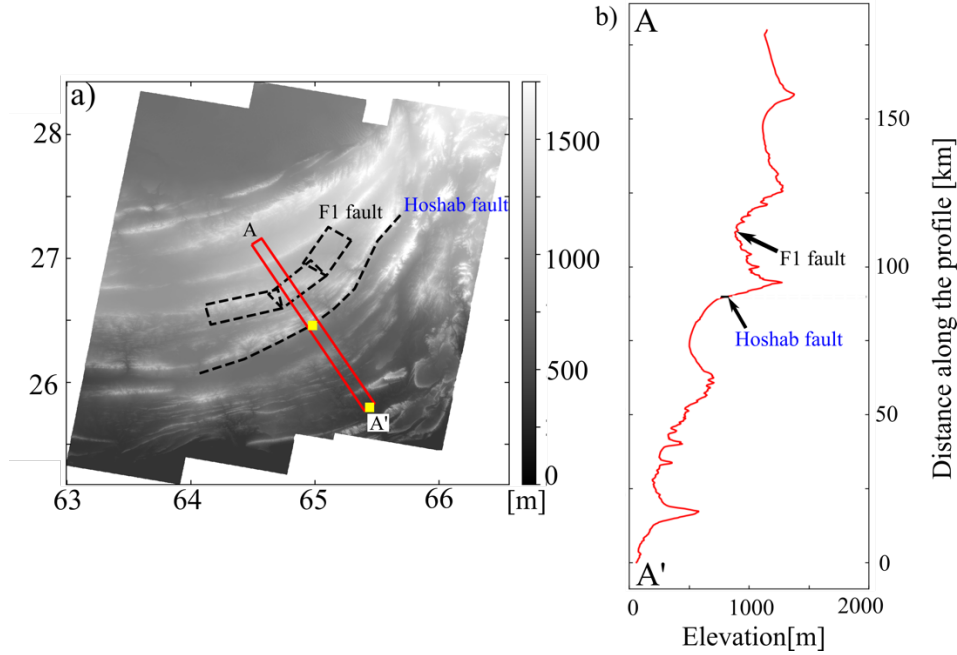


Figure S1.1 Topography profiles perpendicular to the Hoshab fault. Black dashed line: surface trace of Hoshab fault. Black dashed rectangle: F1 fault. Red solid rectangle: profile. Yellow points: two points used for Figure S1.2.

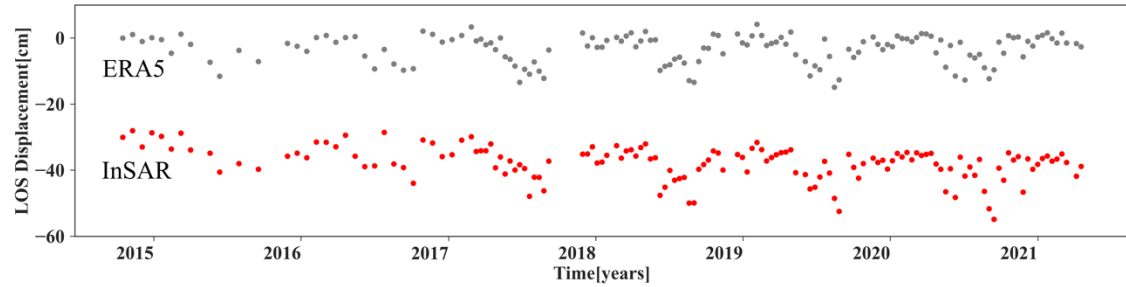


Figure S1.2 InSAR LOS range change time series (red points, after correcting topography error and solid earth tide phase) between two points and the relative time series of tropospheric delay from ERA5 (gray points) between the two points (locations at [25.80N, 65.44E] and [26.46N, 64.98E], elevation difference of 970 m). A constant offset was added to InSAR LOS change data to separate the data.

S2. InSAR Data

Figure S2.1 shows the cumulative displacement from December 2014 to April 2021 of ascending data without removing ramps. Figure S2.2 displays the seams in the overlap areas after concatenation. For the descending data they are caused by three reasons. One is that we use the median of the displacement differences as constant offset, which induces errors because of differences of the displacement difference from the median value; the second one is that the errors of the two swaths are different; the third one is

that same ground displacements can cause different range change in the two swath because of the different radar incidence angles. Figure S2.3 shows the cumulative displacement for the whole time period.

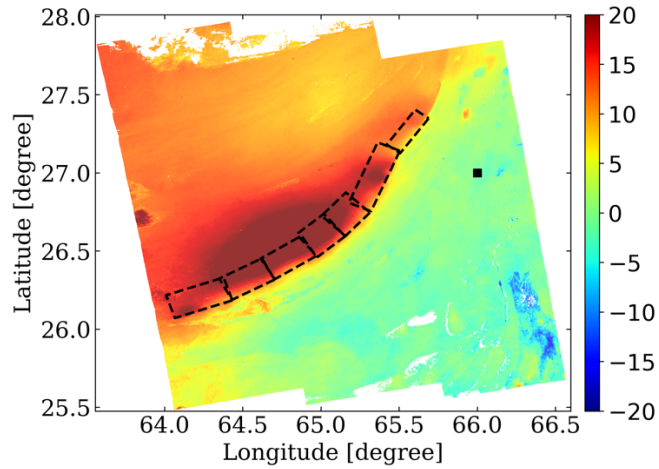


Figure S2.1 Cumulative displacement from December 2014 to April 2021 of ascending data without removing ramps.

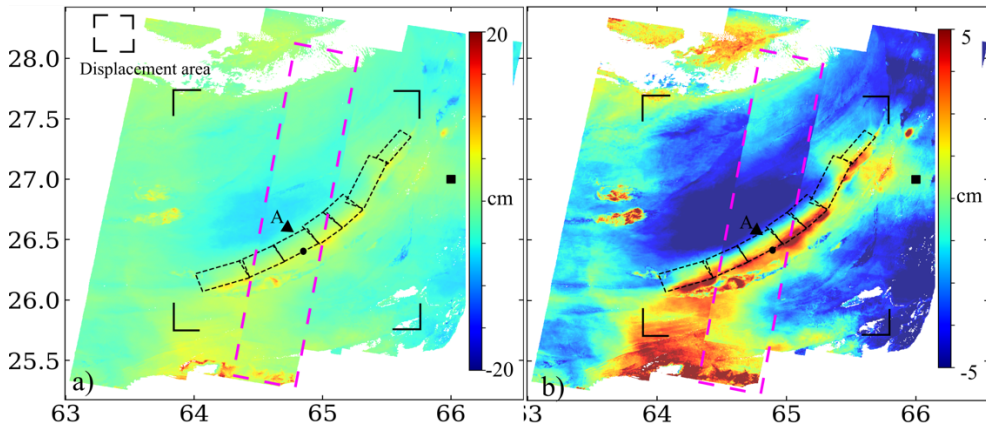


Figure S2.2 (a, b) Two descending swaths displayed using two different colorbars. Pink dashed rectangle: overlap region.

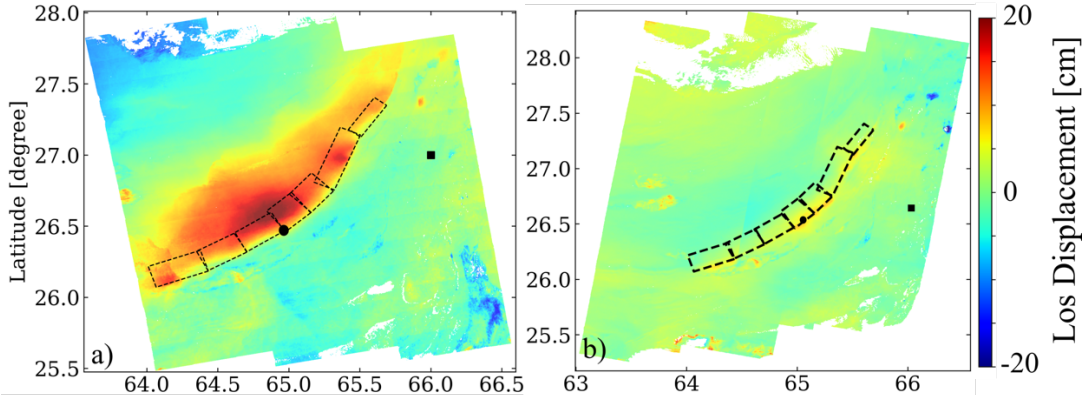


Figure S2.3 a) Ascending and b) descending cumulative post-seismic deformation from December 2014 to April 2021. Black solid square: reference point. Black dashed rectangle in (a), (b): coseismic fault. Black dot: upper edge of the fault.

S3. Detail results of viscoelastic relaxation models

S3.1 Results of viscoelastic relaxation models

We consider linear Maxwell rheology and power-law rheology with powers of 2 and 3.5. The parameters to be estimated are the thickness of the upper accretionary prism and the viscosity of the lower accretionary prism. We use the grid search method to find the best-fitting parameters of the three rheological bodies for time period 1 and time period 2, respectively. The grid search results for time period 1 and time period 2 are shown in Figure S3.1 and Figure S3.2, respectively. The best-fitting parameters of power law rheology with $n=3.5$ are $H=14 \text{ km}$ and $\eta = 10^{18.75} \text{ Pa} \cdot \text{s}$ for both time periods. The best-fitting model of power law rheology with $n=3.5$ is shown in Figure 2b and Figure 2m for time period 1 and time period 2, respectively. Figure S3.3 and S3.4 show the best-fitting model of power law rheology with $n=2$ and linear body for time period 1 and time period 2, respectively.

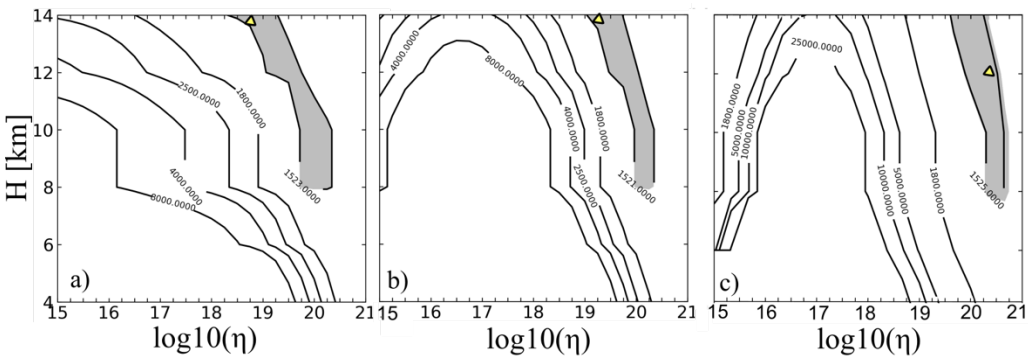


Figure S3.1. Misfit contour map in H and η space of time period 1 for (a) power-law body with $n=3.5$, (b) power-law body with $n=2$ and (c) linear body. The yellow triangles

are the best estimated model in Figure 2b and Figure S3.3, respectively. The gray-shaded area denotes 90% confidence interval calculated using F-Test (Stein and Gordon, 1984).

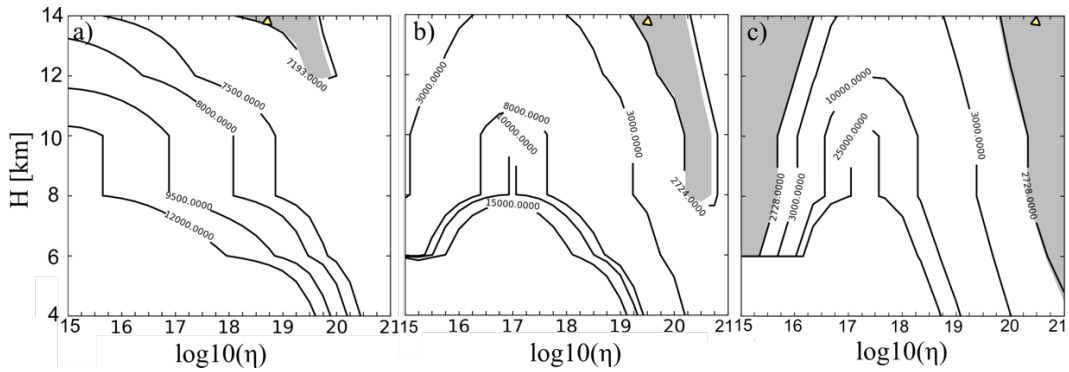


Figure S3.2. Same as Figure S3.1 but for time period 2. The yellow triangles are the best estimated model in Figure 2m and Figure S3.4, respectively.

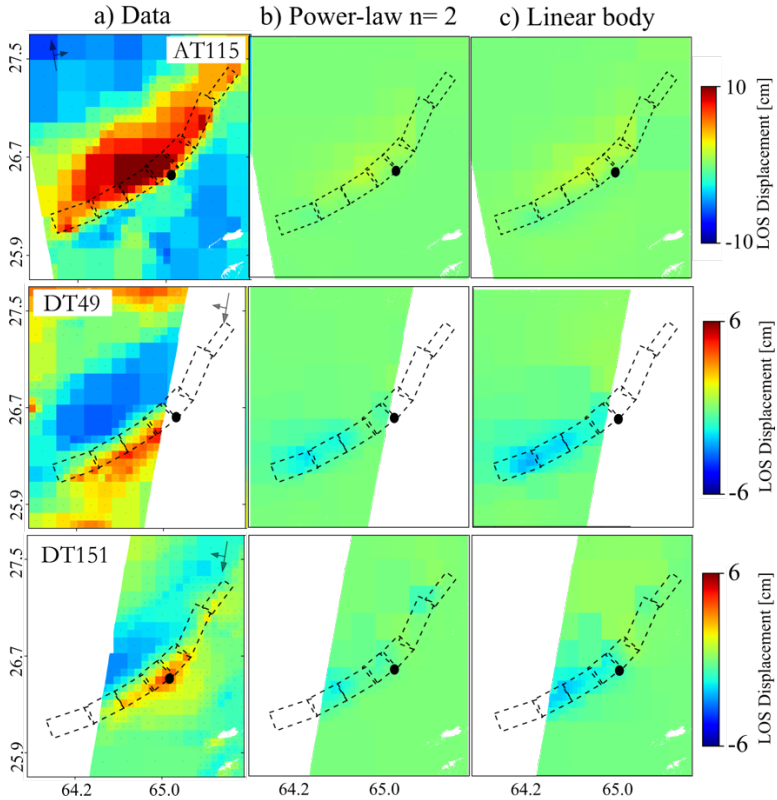


Figure S3.3. Ascending and descending LOS displacements and best-fitting relaxation model results for time period 1. Black dashed rectangle: coseismic fault segments. Black dot: upper edge of the fault.

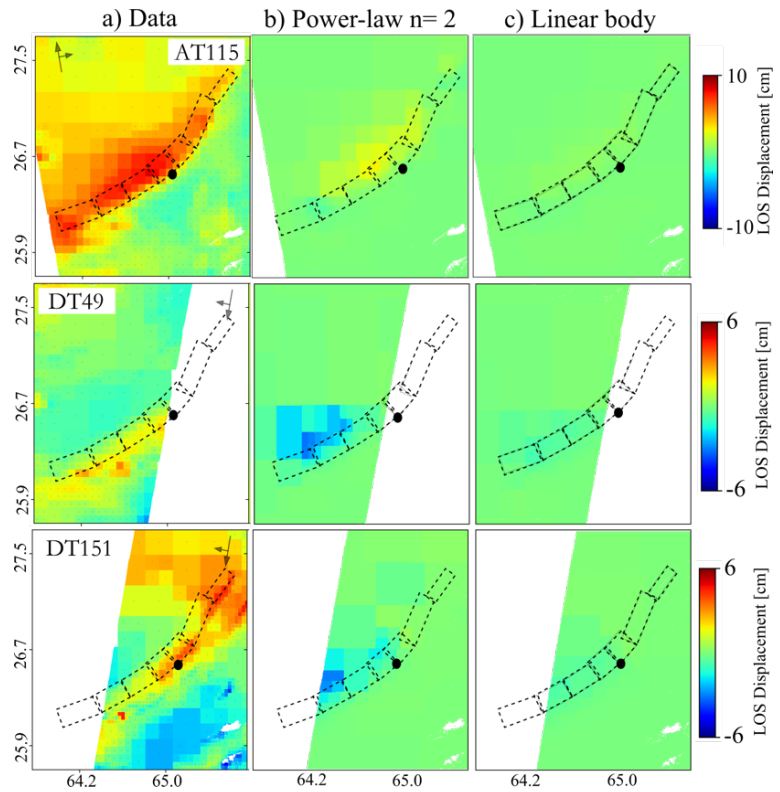


Figure S3.4. Same as Figure S3.3 but for time period 2.

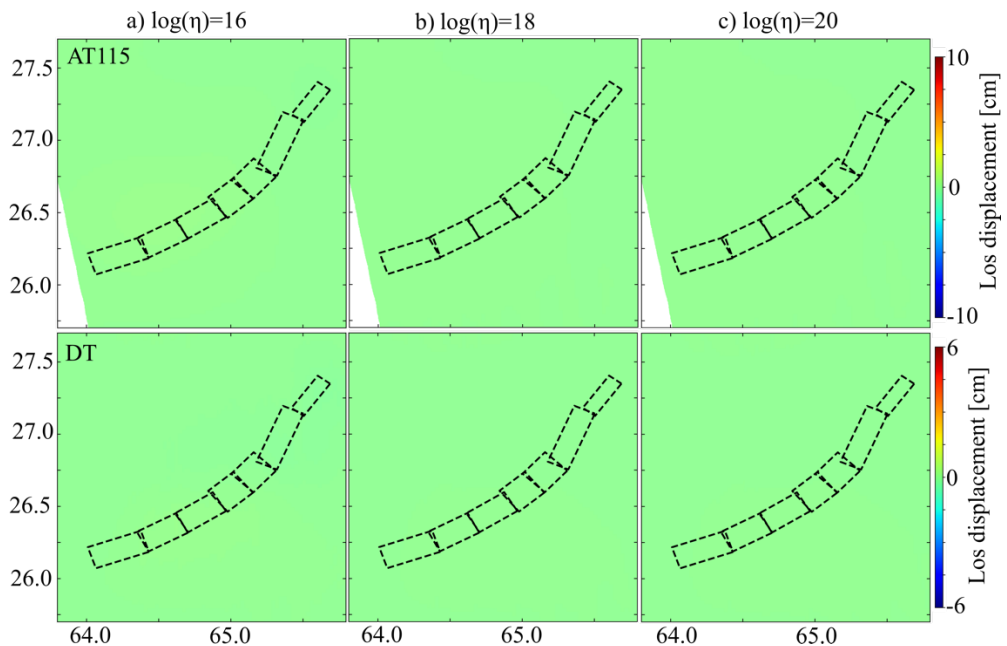


Figure S3.5. Simulated viscoelastic relaxation deformation of ascending and descending data for viscosity equal to $10^{16} \text{ Pa} \cdot \text{s}$, $10^{18} \text{ Pa} \cdot \text{s}$ and $10^{20} \text{ Pa} \cdot \text{s}$, respectively. The

viscoelastic layer ranges from 40 km to 50 km. The dashed rectangles are coseismic dislocation segments.

S3.2. Comparison with Peterson's results

We firstly compare our cumulative displacement (remove ramp from ascending data) ranging from December 2014 to June 2017 with Peterson et al. (2018) (Figure S3.6). One difference between our and the Peterson et al. study is that we correct for the tropospheric delays. Based on the comparison results, we obtain three conclusions. First, our data (Figure S3.6a and S3.6b without tropospheric correction) are very similar to Peterson's result. Next, the blue signal, south of the fault in the ascending data, becomes weak after applying the tropospheric correction (Figure S3.6a and S3.6c). Finally, the blue signal, north of the fault in the descending data, becomes significant after applying the tropospheric correction (Figure S3.6b and S3.6d). Although there are differences between results with and without tropospheric delay correction, the difference is relatively small. Furthermore, as Peterson et al. (2018) state, they accepted the relaxation model which can only grossly explain the observed data, such as the residual at the north of Hoshab fault is almost 4 cm for the descending data.

Next, we compared our cumulative displacement with modeled results using Peterson's best-fitting parameters (Figure S3.7). It can be seen that there is a big discrepancy between the observed data and modeled data.

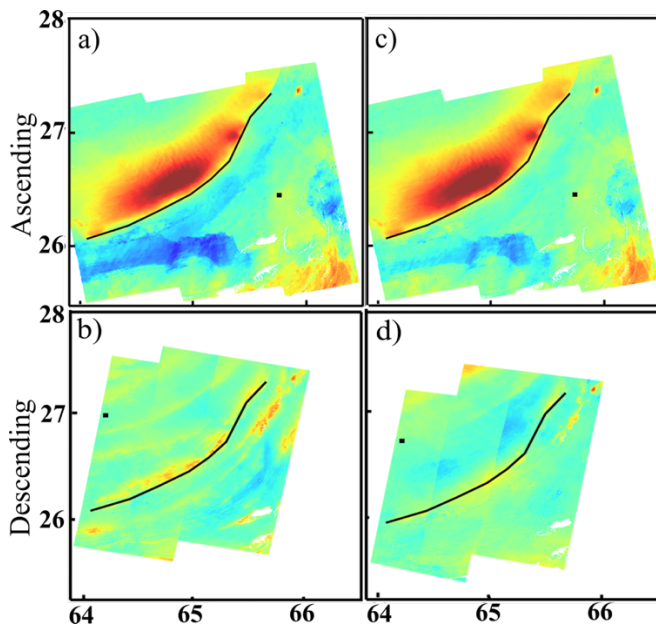


Figure S3.6. (a) Ascending and (b) descending cumulative post-seismic displacements from December 2014 to June 2017 without tropospheric delay correction. (c, d) same as (a, b) but with tropospheric delay correction. Black line: surface trace of Hoshab fault. Black square: reference point.

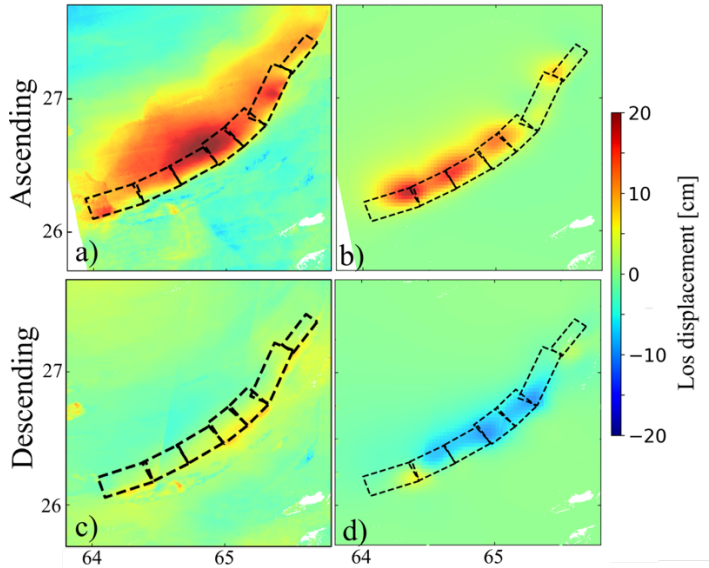


Figure S3.7. (a) ascending and (c) descending observed deformation from Dec 2014 to Apr 2021 and (b, d) simulated viscoelastic relaxation deformation for a model consisting of a 12 km-thick elastic upper accretionary prism overlying a 8 km-thick viscoelastic lower accretionary prism with viscosity of $10^{18} \text{ Pa} \cdot \text{s}$ (best-fitting parameters of Peterson et al. (2018)). The difference between model predictions and observed data show that the viscoelastic model of Peterson does not explain the observations well.

S4. Aseismic slip modelling results of time period 1

Figure S4.1 shows the same as Figure 2a-k but for the original quadtree downsampled results. Figure S4.2 shows the observation-residual results of the down-dip extension model, secondary fault model, basal decollement model, mid-prism decollement model, respectively, for time period 1. Figure S4.3 shows the aseismic slip vector along the decollement faults. Figure S4.4 illustrates the difficulties for separating the three kinds of aseismic slip models only based on the model fitting by showing the vertical and horizontal surface deformation from down-dip extension model, secondary fault model, decollement models.

In the best-fitting down-dip extension model, fault slip occurs between 11 km and 51 km depth with average rake, slip and slip area of 17° , 27 cm and 11000 km^2 respectively (Figure 2c, Figure S4.2b, Table S2.1). For the best-fitting secondary fault model, the depth of the seven coseismic dislocations range from 16 km to 34 km and the depth of the F1 fault from 7 km to 32 km (Figure 2d, Figure S4.2c, Table S2.2). The average rake, slip and slip area of the coseismic and the F1-fault dislocations are 26° , 68 cm and 5300 km^2 , and 11° , 10 cm and 4100 km^2 , respectively.

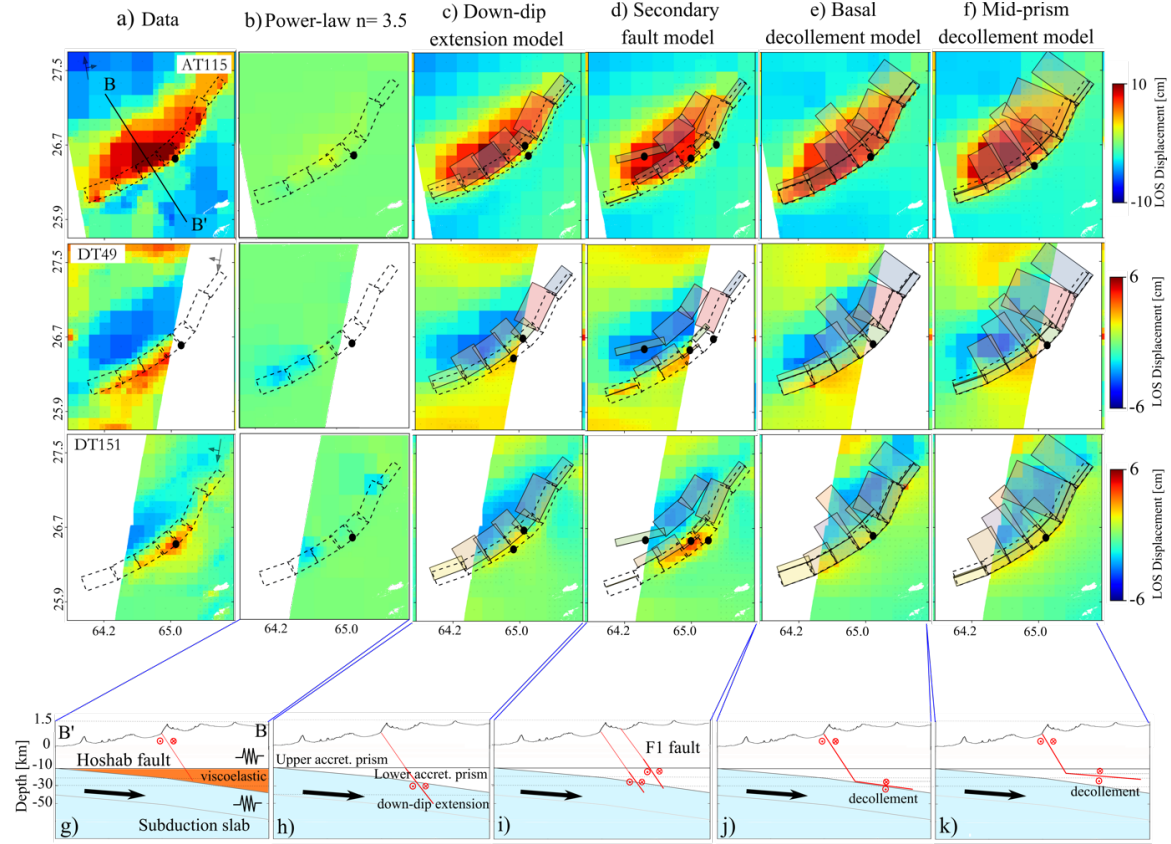


Figure S4.1. Same as Figure 2a-k but for the original quadtree downsampled results.

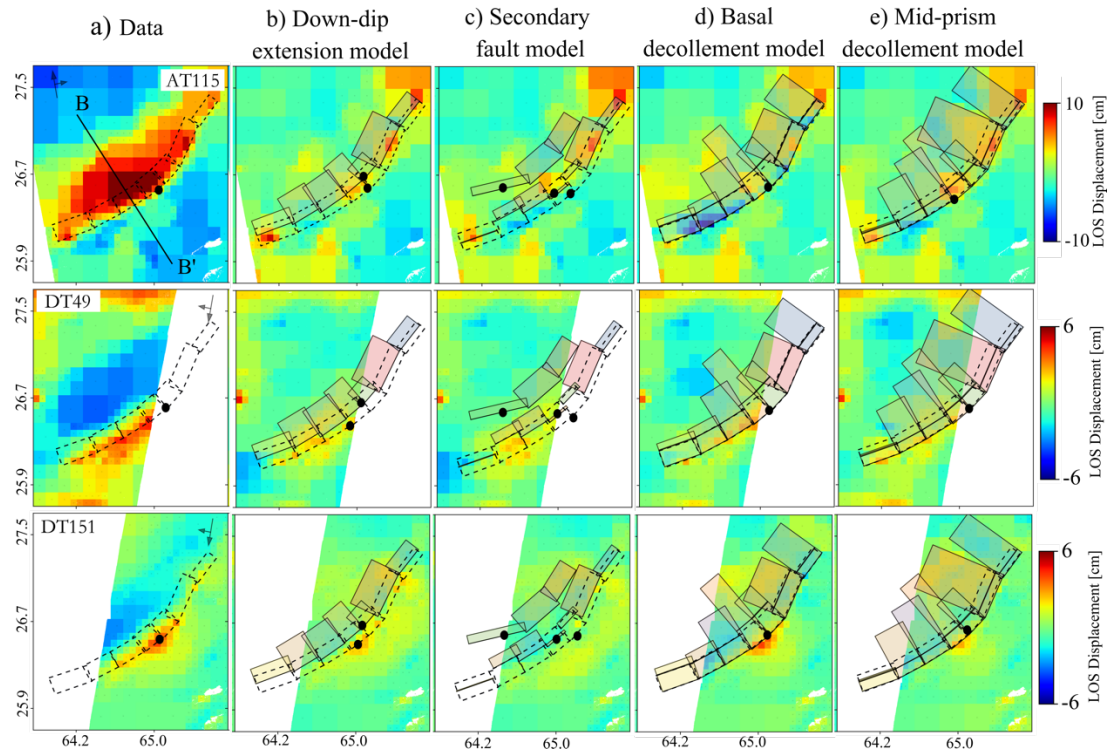


Figure S4.2. (a) Observed LOS displacements of time period 1. Residual of time period 1 for (b) down-dip extension model, (c) secondary fault model, (d) basal decollement model and (e) mid-prism decollement model. In (a) - (e): Black dashed rectangle: coseismic fault segments; black dot: upper edge of the fault; black solid rectangle: aseismic slip faults.

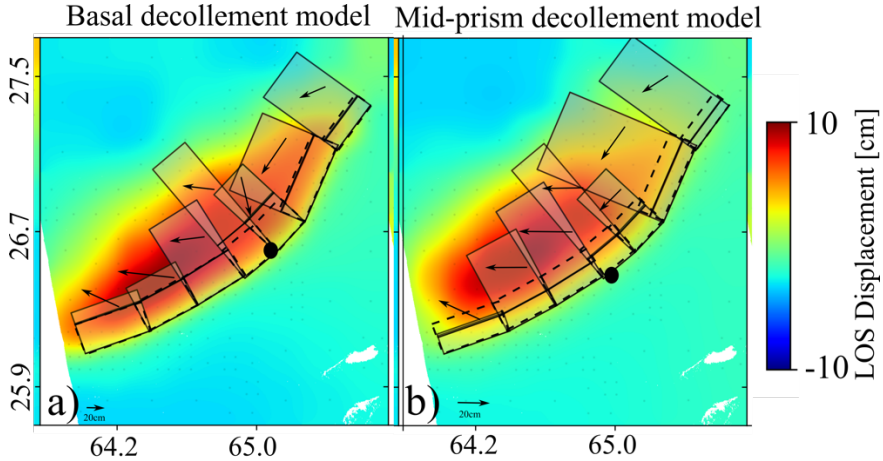


Figure S4.3. Rake and slip magnitude of aseismic slip for (a) basal decollement models and (b) mid-prism decollement model together with the simulated LOS displacements. The black arrows are the slip vector. Other symbols are the same as Figure S4.1.

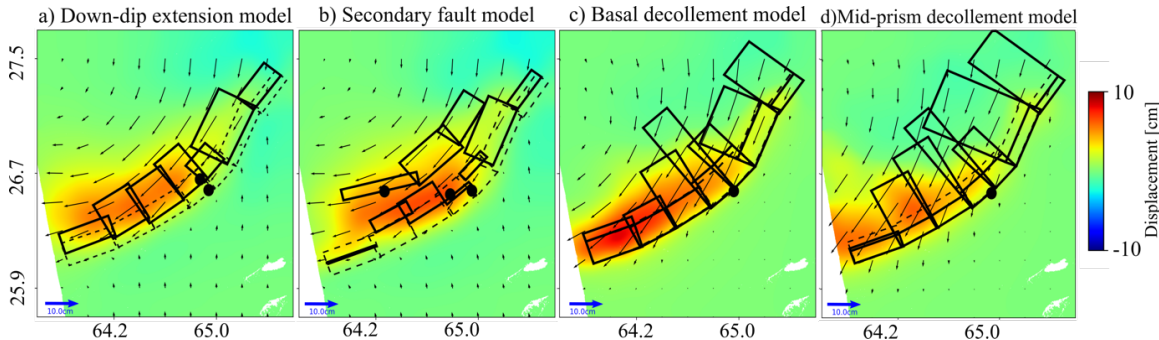


Figure S4.4. Surface deformation from (a) down-dip extension model, (b) secondary fault model, (c) basal decollement model and (d) mid-prism decollement model, illustrating the difficulties for separating these three kinds of models only based on the model fitting. Vectors: horizontal displacements; color shading: vertical displacements. Here interpolations based on the quadtree-downsampled data are shown.

S5. Aseismic slip modelling results of time period 2

Figure S5.1 shows the same as Figure 2l-t but for the original quadtree downsampled results. Figure S5.2 shows the observation-residual results of the down-dip extension model, basal decollement model, mid-prism decollement model, respectively, for time period 2.

In the best-fitting down-dip extension model, fault slip occurs between 12 km and 38 km depth with average rake, slip and slip area of 27° , 23 cm and 7600 km^2 , respectively (Figure 2n, Figure S5.2b, Table S3.1). For the best-fitting basal decollement model, the seven decollement dislocations have average width, dip, rake, slip and slip area of 19.3 km, 6° , 39° , 130 cm and 5000 km^2 respectively, and the average rake and slip of coseismic dislocations are 24° and 1.5 cm (Figure 2o, Figure S5.2c, Table S3.2). For the best-fitting mid-prism decollement model, the average width, dip, rake, slip and slip area of the seven decollements are 46.9 km, 6° , 38° , 18 cm and 11000 km^2 , respectively, and the average rake and slip of coseismic dislocations are 19° and 1.3 cm (Figure 2p, Figure S5.2d, Table S3.3).

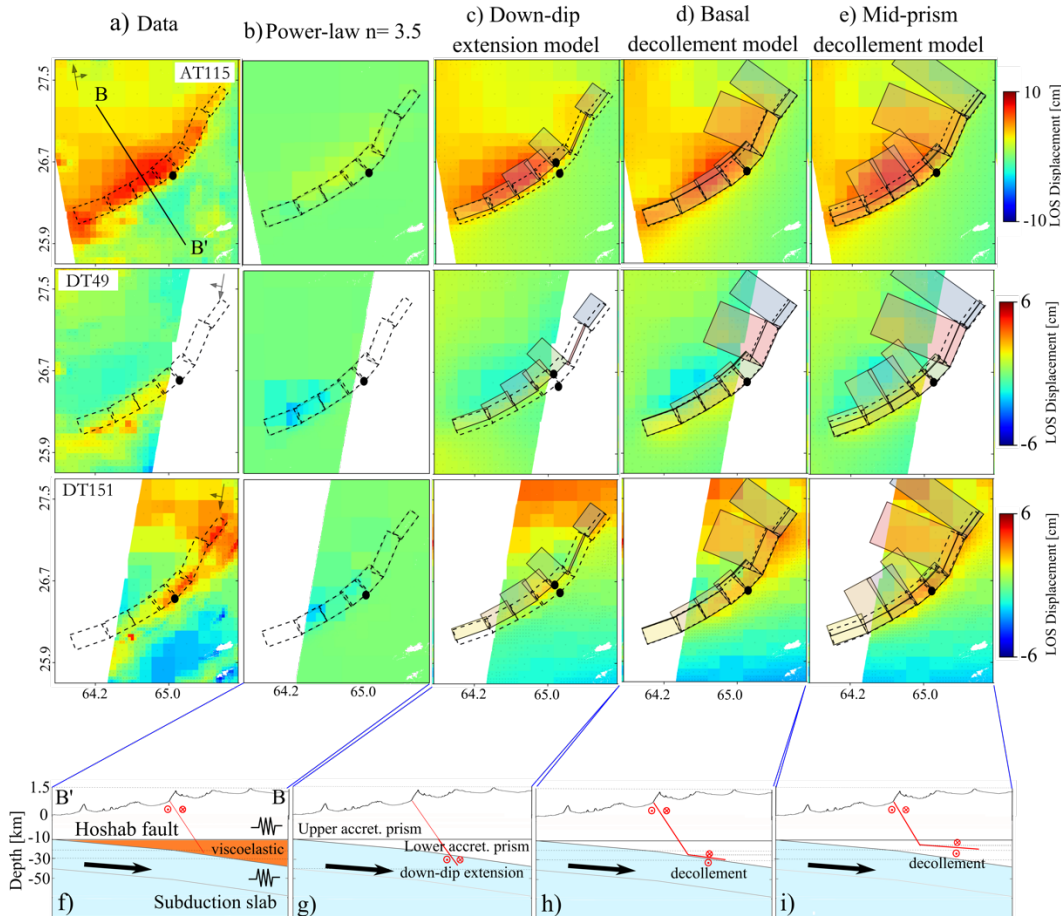


Figure S5.1. Same as Figure 2l-t but for the original quadtree downsampled results.

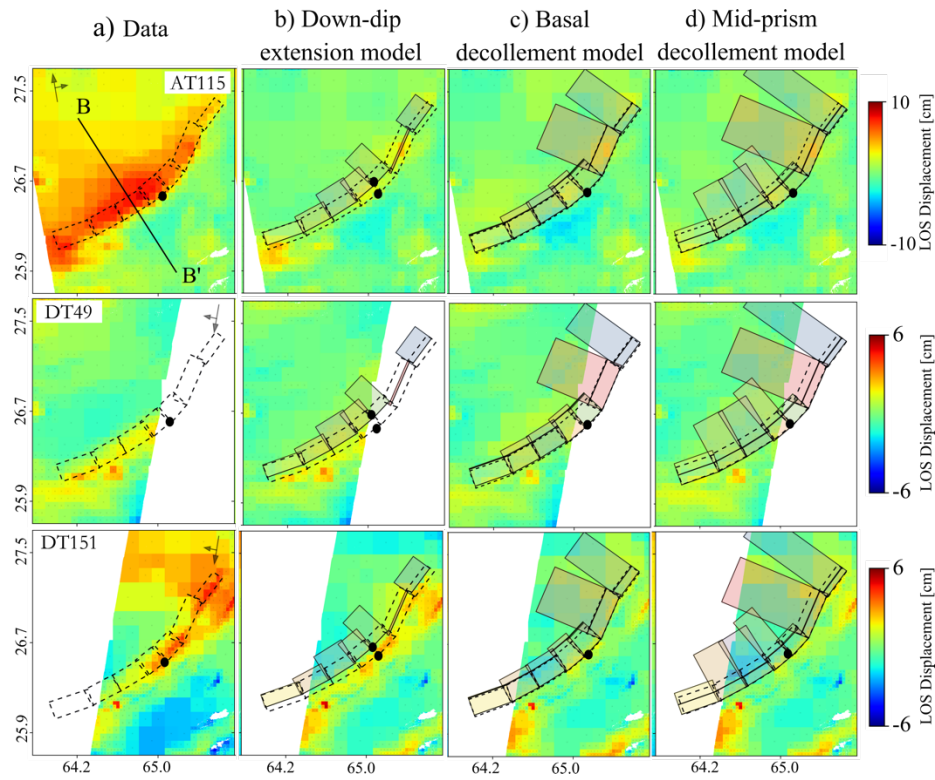


Figure S5.2. Same as Figure S4.2 but for time period 2.

S6. Strength Profile

According to the stratigraphy of Makran, the mainly broad facies in the eastern Makran prism are Talat, Parkini, Panjgure and Hoshab phase, which are composed of the mudstones and sandstones with fine-grained to very fine-grained size (Ellouz-Zimmermann et al., 2007). Mudstones and sandstone are a mixture of quartz and feldspar. The friction coefficients for the out-of-sequence splay faults in the accretionary is $<\sim 0.2$ (Li et al., 2014). The measured average geothermal gradients by the drilled well located at Kech Band and its southern region is $20^{\circ}\text{C}/\text{km}$ (Khan et al., 1986). Besides $20^{\circ}\text{C}/\text{km}$, $25^{\circ}\text{C}/\text{km}$ and $30^{\circ}\text{C}/\text{km}$ are also used to calculate strength profile. It can be concluded that the accretionary prism shows elastic behavior even if the geothermal gradient reaches to $30^{\circ}\text{C}/\text{km}$.

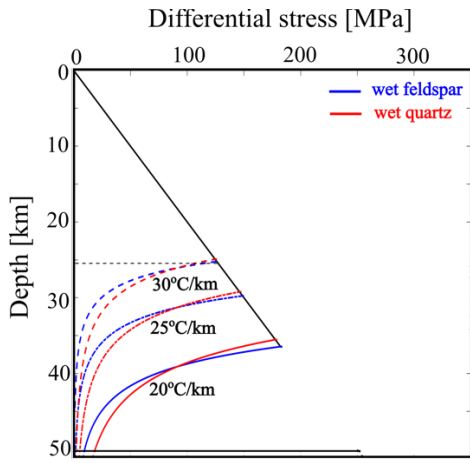


Figure S6. Strength envelope plot for the Makran accretionary prism assuming a strain rate of $10^{-14}s^{-1}$. The grain size and the friction coefficient are 50 um and 0.2, respectively. The geothermal gradients are 20°C/km, 25°C/km, 30°C/km, respectively. The black dashed horizontal line is the bottom edge of the prism.

S7. Coulomb stress change results

Figure S7.1 and Figure S7.2 shows the coulomb stress change on the best-fitting aseismic slip models imparted by the coseismic fault with effective friction coefficient of 0 and 0.7, respectively. Figure S7.3 shows the direction of maximum coseismic shear stress and aseismic slip for the (a) basal decollement model and (b) mid-prism decollement model for time period 2. Figure S7.4 shows how the RMSE and shear stress changes with aseismic slip rake for basal decollement model and mid-prism decollement model. The rake range is $[-90^\circ, 90^\circ]$ with a step of 10° . It can be seen that the shear stress gets to the peak when the rake is equal to 10° both for the basal decollement model and mid-prism decollement model. And the RMSE gets biggest when the rake angle is close to the 90° or -90° and the smallest RMSE is obtained at rake = 20° , both of them indicate that the inverted aseismic slip rake angle is well constrained.

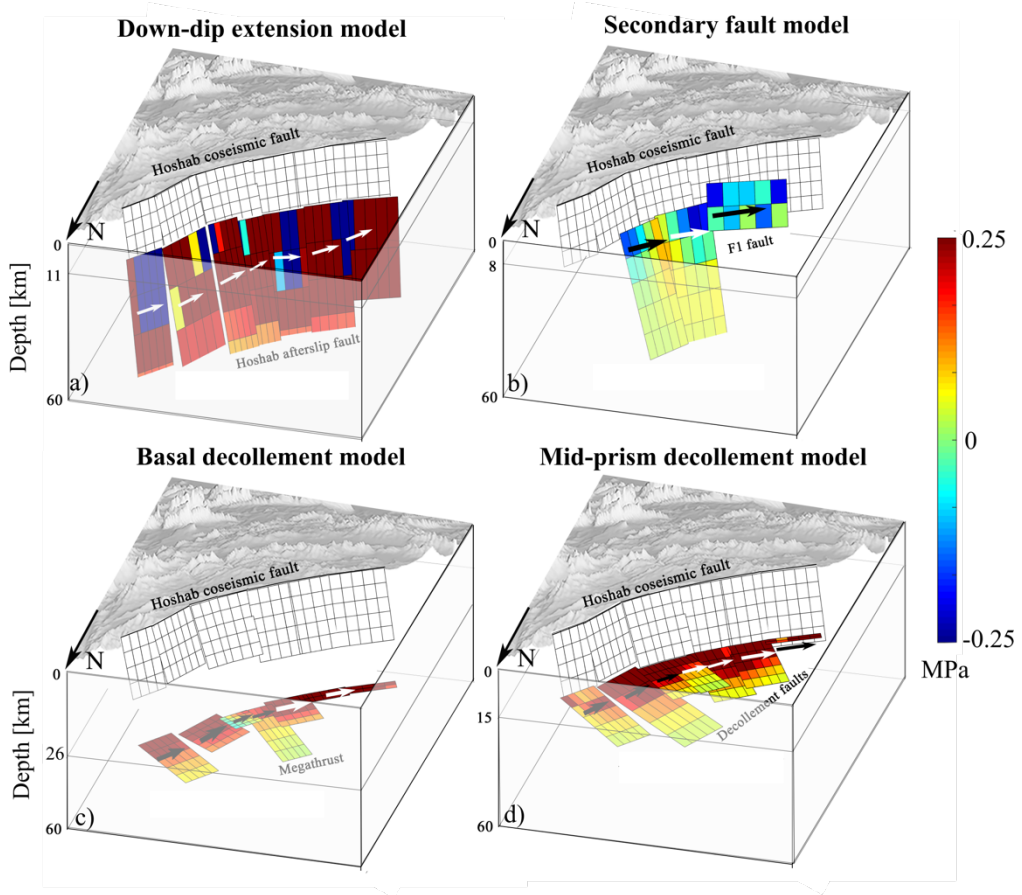


Figure S7.1. Same as Figure 3 but for an effective friction coefficient of 0.

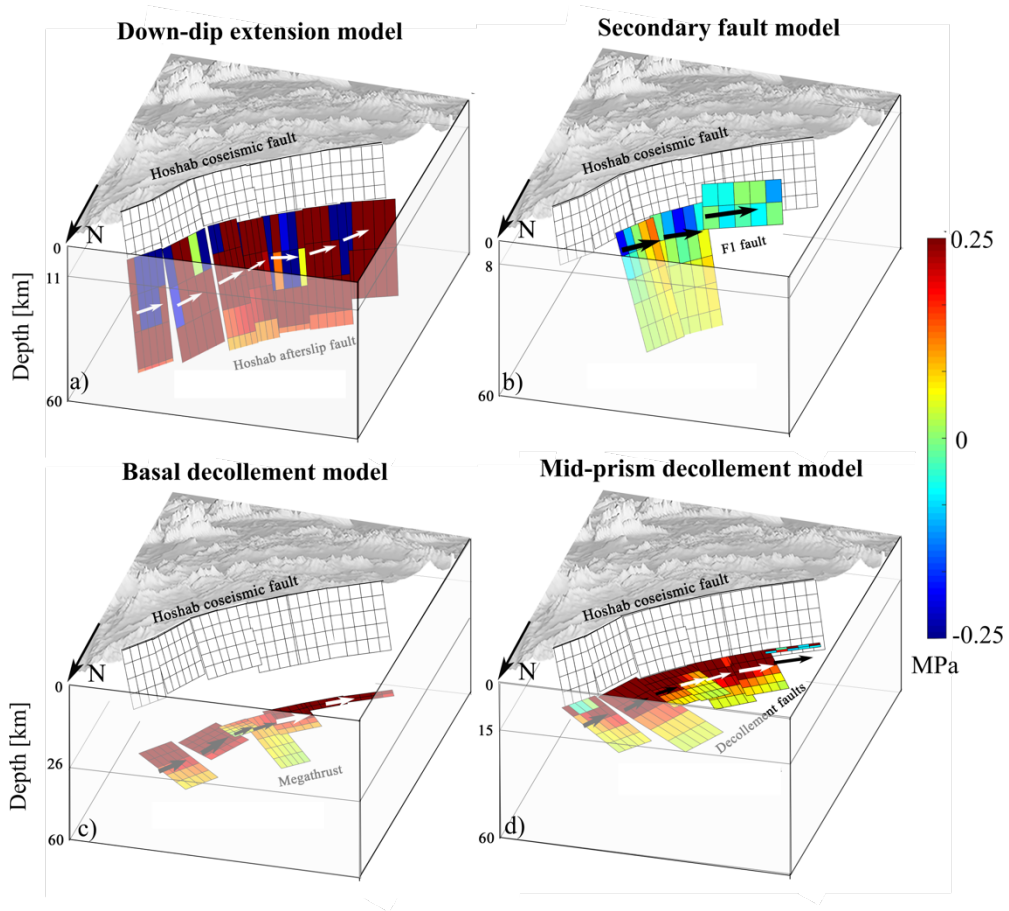


Figure S7.2. Same as Figure 3 but for an effective friction coefficient of 0.7.

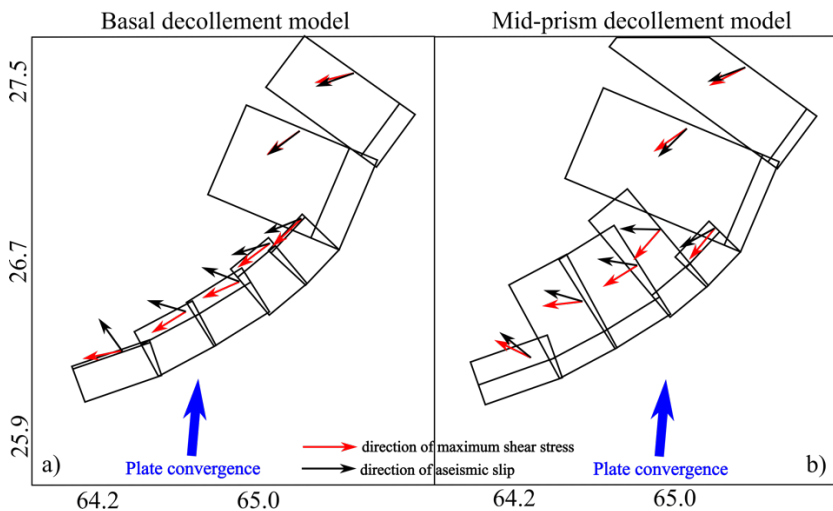


Figure S7.3 Direction of maximum coseismic shear stress, aseismic slip and plate convergence for the (a) basal decollement model and (b) mid-prism decollement model for time period 2. The arrow length are shown with unit length.

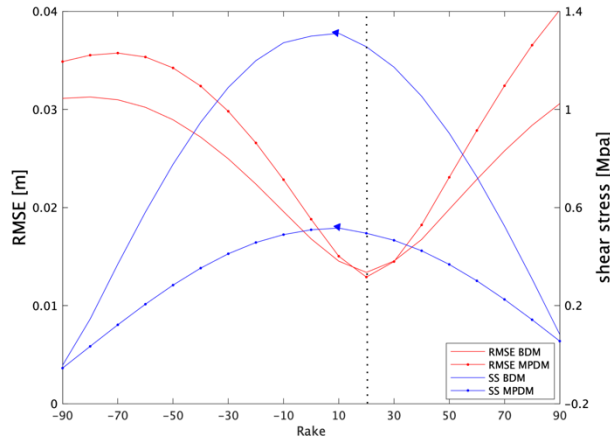


Figure S7.4. The relationship between average RMSE, average shear stress with aseismic slip rake for basal decollement model and mid-prism decollement model for the whole time period. The dashed thin black line: inverted average aseismic slip rake. The blue triangles: rake angle having the maximum shear stress.

S8. Summary of tables

Table S1 is the summary of aseismic slip and relaxation models in this paper. Table S2.1, Table S2.2, Table S2.3 and Table S2.4 show the range, optimal and uncertainties of InSAR-inversion fault slip parameters of the down-dip extension model, secondary fault model, basal decollement model and mid-prism decollement model, respectively, for time period 1. Table S3.1, Table S3.2 and Table S3.2 show the range, optimal and uncertainties of InSAR-inversion fault slip parameters of the down-dip extension model, basal decollement model and mid-prism decollement model, respectively, for time period 2. Table S4 shows the direction (rake) of maximum coseismic shear stress and aseismic slip of basal decollement model and mid-prism decollement model for time period 1 and time period 2, respectively. We use the Aki and Richards convention.

	Time period 1			Time period 2		
	aseismic slip models					
	RMSE (m)	Inversion table	Data- residual fig.	RMSE (m)	Inversion table	Data- residual fig.
Down-dip extension model	0.015	Table S2.1	Figure S4.2b	0.012	Table S3.1	Figure S5.2b
Secondary fault model	0.014	Table S2.2	Figure S4.2c	—	—	—
Basal decollement model	0.015	Table S2.3	Figure S4.2d	0.011	Table S3.2	Figure S5.2c

Mid-prism decollement model	0.014	Table S2.4	Figure S4.2e	0.010	Table S3.3	Figure S5.2d
Viscoelastic models						
	RMSE(m)	Misfit-contour fig.	Data- model fig.	RMSE(m)	Misfit- contour fig.	Data- model fig.
Power law = 3.5	0.039	Figure S3.1a	Figure 2b	0.022	Figure S3.2a	Figure 2m
Power law = 2	0.040	Figure S3.1b	Figure S3.3b	0.023	Figure S3.2b	Figure S3.4b
Linear body	0.042	Figure S3.1c	Figure S3.3c	0.023	Figure S3.2c	Figure S3.4c

Table S1. Summary of aseismic slip models and viscoelastic relaxation models.

	Length (km)	Width (km)	Depth (km)	Dip (°)	Strike (°)	Rake (°)	Net slip (m)	lat	lon	Mw	Rms (m)
Coseismic segment 1											
Lower	48	0	0	60	203	-90	0	27.16	65.48	7.33	0.015
Upper	same	70	20	Same as above		90	1.5				
Optimal	--	57.9	11.3	--	--	8.4	0.37				
2.5%	--	52.9	5.2	--	--	0.4	0.25				
97.5%	--	63.7	15.8	--	--	18.6	0.48				
Coseismic segment 2											
Lower	32	0	0	70	216	-90	0	65.68	27.37		
Upper	same	70	20	Same as above		90	1.5				
Optimal	--	49.5	11.2	--	--	12.4	0.40				
2.5%	--	35.1	7.2	--	--	3.2	0.26				
97.5%	--	62.3	15.6	--	--	23.5	0.53				
Coseismic segment 3											
Lower	24	0	0	47	223	-90	0	65.25	26.80		
Upper	same	70	20	Same as above		90	1.5				
Optimal	--	45.9	10.3	--	--	-1.4	0.16				
2.5%	--	13.2	3.5	--	--	-39.8	0.01				
97.5%	--	69.1	19.9	--	--	33.7	0.33				
Coseismic segment 4											
Lower	24	0	0	47	230	-90	0	65.11	26.65		
Upper	same	70	20	Same as above		90	1.5				
Optimal	--	54.6	11.4	--	--	37.4	0.27				
2.5%	--	43.5	5.8	--	--	14.2	0.14				
97.5%	--	67.6	18.1	--	--	70.5	0.40				
Coseismic segment 5											
Lower	32	0	0	56	238	-90	0	64.94	26.51		
Upper	same	70	20	Same as above		90	1.5				
Optimal	--	54.9	11.3	--	--	17.3	0.37				
2.5%	--	44.6	3.7	--	--	4.2	0.23				
97.5%	--	65.8	18.9	--	--	32.6	0.50				
Coseismic segment 6											

Lower	32	0	0	56	242	-90	0	64.66	26.38
Upper	same	70	20	Same as above		90	1.5		
Optimal	--	51.7	10.7	--	--	8.3	0.26		
2.5%	--	32.2	4.3	--	--	-5.3	0.14		
97.5%	--	68.2	19.7	--	--	22.6	0.39		
Coseismic segment 7									
Lower	40	0	0	56	251	-90	0	64.42	26.25
Upper	same	70	20	Same as above		90	1.5		
Optimal	--	28.2	10.6	--	--	33.8	0.05		
2.5%	--	5.0	3.1	--	--	1.4	0		
97.5%	--	58.6	15.7	--	--	53.3	0.14		

Table S2.1. Range, optimal and uncertainties of InSAR-inversion fault slip parameters of the down-dip extension model for time period 1.

	Length (km)	Width (km)	Depth (km)	Dip (°)	Strike (°)	Rake (°)	Net slip (m)	lat	lon	Mw	Rms (m)
Coseismic segment 1											
Lower	48	0	0	60	203	-90	0	27.16	65.50	7.33	0.014
Upper	same	70	25	Same as above		90	5.0				
Optimal	--	46.3	17.5	--	--	7.2	0.43				
2.5%	--	27.6	9.4	--	--	-3.8	0.22				
97.5%	--	55.1	24.9	--	--	20.1	0.64				
Coseismic segment 2											
Lower	32	0	0	70	216	-90	0	27.37	65.68		
Upper	same	70	25	Same as above		90	5.0				
Optimal	--	36.3	17.9	--	--	14.3	0.61				
2.5%	--	21.8	12.3	--	--	4.6	0.30				
97.5%	--	52.1	23.2	--	--	25.3	0.93				
Coseismic segment 3											
Lower	24	0	0	47	223	-90	0	26.80	65.25		
Upper	same	70	25	Same as above		90	5.0				
Optimal	--	11.7	16.8	--	--	-0.1	0.58				
2.5%	--	0.6	12.2	--	--	-41.6	0.23				
97.5%	--	29.8	20.1	--	--	40.3	1.18				
Coseismic segment 4											
Lower	24	0	0	47	230	-90	0	26.63	65.10		
Upper	same	70	25	Same as above		90	5.0				
Optimal	--	4.4	18.1	--	--	58.2	1.08				
2.5%	--	0.1	13.7	--	--	34.6	0.0				
97.5%	--	9.2	23.4	--	--	83.9	2.73				
Coseismic segment 5											
Lower	32	0	0	56	238	-90	0	26.49	64.93		
Upper	same	70	25	Same as above		90	5.0				
Optimal	--	28.9	19.2	--	--	42.9	0.53				
2.5%	--	12.1	16.4	--	--	21.1	0.26				

97.5%	--	44.6	24.9	--	--	75.1	0.85		
Coseismic segment 6									
Lower	32	0	0	56	242	-90	0	26.41	64.69
Upper	same	70	25	Same as above		90	5.0		
Optimal	--	17.3	14.0	--	--	1.3	0.58		
2.5%	--	7.6	9.1	--	--	-16.4	0.26		
97.5%	--	27.3	19.2	--	--	18.1	1.07		
Coseismic segment 7									
Lower	40	0	0	56	251	-90	0	26.19	64.41
Upper	same	70	25	Same as above		90	5.0		
Optimal	--	1.7	9.1	--	--	54.9	0.99		
2.5%	--	0.3	7.7	--	--	38.4	0.59		
97.5%	--	4.3	11.6	--	--	77.7	1.56		
F1 segment 1									
Lower	38	0	0	47	212	-90	0	27.18	65.24
Upper	same	70	15	Same as above		90	5.0		
Optimal	--	40.9	9.0	--	--	6.3	0.10		
2.5%	--	25.4	7.0	--	--	-19.1	0.00		
97.5%	--	53.6	9.9	--	--	34.5	0.20		
F1 segment2									
Lower	45	0	0	56	229	-90	0	26.88	65.07
Upper	same	70	15	Same as above		90	5.0		
Optimal	--	40.6	8.9	--	--	5.8	0.14		
2.5%	--	13.6	5.7	--	--	-16.1	0.00		
97.5%	--	67.9	11.6	--	--	28.1	0.25		
F1 segments3									
Lower	60	0	0	56	257	-90	0	26.63	64.73
Upper	same	70	15	Same as above		90	5.0		
Optimal	--	13.5	3.9	--	--	21.9	0.07		
2.5%	--	0.01	0.0	--	--	-14.9	0.00		
97.5%	--	32.7	8.9	--	--	61.5	0.23		

Table S2.2. Same as Table S2.1 but for the secondary fault model of time period 1.

	Length (km)	Width (km)	Depth (km)	Dip (°)	Strike (°)	Rake (°)	Net slip (m)	lat	lon	Mw	Rms (m)
Coseismic segment 1											
Lower	48	30.0	0	60	203	-90	0	27.1	65.6		7.34
Upper		Same as above				90	5.0				0.015
Optimal	--	--	--	--	--	3.6	0.104				
2.5%	--	--	--	--	--	-5.0	0.100				
97.5%	--	--	--	--	--	12.0	0.110				
Coseismic segment 2											
Lower	32	27.7	0	70	216	-90	0	27.3	65.7		
Upper		Same as above				90	5.0				
Optimal	--	--	--	--	--	15.8	0.104				
2.5%	--	--	--	--	--	4.4	0.100				
97.5%	--	--	--	--	--	27.5	0.120				

Coseismic segment 3								
Lower	24	35.6	0	47	223	-90	0	26.7 65.3
Upper		Same as above				90	5.0	
Optimal	--	--	--	--	--	22.9	0.105	
2.5%	--	--	--	--	--	15.3	0.100	
97.5%	--	--	--	--	--	29.1	0.120	
Coseismic segment 4								
Lower	24	35.6	0	47	230	-90	0	26.6 65.2
Upper		Same as above				90	5.0	
Optimal	--	--	--	--	--	37.9	0.103	
2.5%	--	--	--	--	--	31.1	0.100	
97.5%	--	--	--	--	--	44.8	0.110	
Coseismic segment 5								
Lower	32	31.4	0	56	238	-90	0	26.5 64.9
Upper		Same as above				90	5.0	
Optimal	--	--	--	--	--	31.3	0.103	
2.5%	--	--	--	--	--	22.4	0.100	
97.5%	--	--	--	--	--	39.6	0.110	
Coseismic segment 6								
Lower	32	31.4	0	56	242	-90	0	26.3 64.7
Upper		Same as above				90	5.0	
Optimal	--	--	--	--	--	35.9	0.102	
2.5%	--	--	--	--	--	26.9	0.100	
97.5%	--	--	--	--	--	44.5	0.108	
Coseismic segment 7								
Lower	40	31.4	0	56	251	-90	0	26.2 64.4
Upper		Same as abve				90	5.0	
Optimal	--	--	--	--	--	49.5	0.102	
2.5%	--	--	--	--	--	38.3	0.100	
97.5%	--	--	--	--	--	61.9	0.109	
Decollement segment 1								
Lower	48	0	26	0	203	-90	0	27.2 65.4
Upper	same	70	same	10	same	90	8.0	
Optimal	--	27.6	--	7.3	--	10.4	0.31	
2.5%	--	17.1	--	3.6	--	-0.45	0.23	
97.5%	--	36.4	--	9.9	--	21.3	0.42	
Decollement segment 2								
Lower	32	0	26	0	216	-90	0	27.4 65.6
Upper	same	70	same	10	same	90	8.0	
Optimal	--	47.1	--	8.1	--	28.9	0.31	
2.5%	--	37.2	--	4.6	--	16.6	0.19	
97.5%	--	60.0	--	9.9	--	42.2	0.43	
Decollement segment 3								
Lower	24	0	26	0	223	-90	0	26.9 65.1
Upper	same	70	same	10	same	90	8.0	
Optimal	--	19.8	--	3.5	--	-17.2	0.42	
2.5%	--	7.3	--	0.0	--	-39.8	0.10	
97.5%	--	30.8	--	8.3	--	26.5	1.50	
Decollement segment 4								
Lower	24	0	26	0	230	-90	0	26.8 65.0
Upper	same	70	same	10	same	90	8.0	
Optimal	--	55.4	--	8.4	--	53.7	1.79	
2.5%	--	46.5	--	5.1	--	35.6	0.67	

97.5%	--	63.3	--	9.9	--	71.3	3.18		
Decollement segment 5									
Lower	32	0	26	0	238	-90	0	26.6	64.9
Upper	same	70	same	10	same	90	8.0		
Optimal	--	33.7	--	5.1	--	24.5	0.28		
2.5%	--	21.8	--	0.1	--	5.3	0.19		
97.5%	--	45.3	--	9.9	--	42.4	0.38		
Decollement segment 6									
Lower	32	0	26	0	242	-90	0	26.4	64.6
Upper	same	70	same	10	same	90	8.0		
Optimal	--	10.8	--	5.3	--	33.3	0.18		
2.5%	--	2.6	--	0.1	--	6.1	0.10		
97.5%	--	18.7	--	5.6	--	60.4	0.27		
Decollement segment 7									
Lower	40	0	26	0	251	-90	0	26.2	64.4
Upper	same	70	same	10	same	90	8.0		
Optimal	--	8.0	--	5.5	--	51.9	0.22		
2.5%	--	1.1	--	0.3	--	35.9	0.10		
97.5%	--	16.8	--	9.7	--	69.8	0.37		

Table S2.3. Same as Table S2.1 but for basal decollement model of time period 1.

	Length (km)	Width (km)	Depth (km)	Dip (°)	Strike (°)	Rake (°)	Net slip (m)	lat	lon	Mw	Rms (m)
Coseismic segment 1										7.28	0.014
Lower	48	30.0	0	60	203	-90	0	27.1	65.6		
Upper		Same as above				90	5.0				
Optimal	--	--	--	--	--	1.9	0.04				
2.5%	--	--	--	--	--	-24.3	0				
97.5%	--	--	--	--	--	25.2	0.07				
Coseismic segment 2											
Lower	32	27.7	0	70	216	-90	0	27.3	65.7		
Upper		Same as above				90	5.0				
Optimal	--	--	--	--	--	8.4	0.02				
2.5%	--	--	--	--	--	-20.1	0				
97.5%	--	--	--	--	--	33.7	0.05				
Coseismic segment 3											
Lower	24	35.6	0	47	223	-90	0	26.7	65.3		
Upper		Same as above				90	5.0				
Optimal	--	--	--	--	--	14.7	0.03				
2.5%	--	--	--	--	--	-18.5	0				
97.5%	--	--	--	--	--	37.9	0.07				
Coseismic segment 4											
Lower	24	35.6	0	47	230	-90	0	26.6	65.2		
Upper		Same as above				90	5.0				
Optimal	--	--	--	--	--	11.6	0.01				
2.5%	--	--	--	--	--	-18.9	0				
97.5%	--	--	--	--	--	59.6	0.03				
Coseismic segment 5											
Lower	32	31.4	0	56	238	-90	0	26.5	64.9		
Upper		Same as above				90	5.0				
Optimal	--	--	--	--	--	6.4	0.01				
2.5%	--	--	--	--	--	-20.9	0				

97.5%	--	--	--	--	--	32.3	0.03		
Coseismic segment 6									
Lower	32	31.4	0	56	242	-90	0	26.3	64.7
Upper		Same as above				90	5.0		
Optimal	--	--	--	--	--	-11.3	0.006		
2.5%	--	--	--	--	--	-49.7	0		
97.5%	--	--	--	--	--	44.2	0.02		
Coseismic segment 7									
Lower	40	31.4	0	56	251	-90	0	26.2	64.4
Upper		Same as abve				90	5.0		
Optimal	--	--	--	--	--	37.6	0.03		
2.5%	--	--	--	--	--	-4.2	0		
97.5%	--	--	--	--	--	69.6	0.06		
Decollement segment 1									
Lower	48	0	15	0	203	-90	0	27.2	65.4
Upper	same	100	same	10	same	90	8.0		
Optimal	--	72.5	--	8.2	--	13.4	0.25		
2.5%	--	61.8	--	6.5	--	5.1	0.19		
97.5%	--	81.9	--	9.9	--	22.2	0.32		
Decollement segment 2									
Lower	32	0	15	0	216	-90	0	27.4	65.6
Upper	same	100	same	10	same	90	8.0		
Optimal	--	57.1	--	8.3	--	19.1	0.18		
2.5%	--	38.9	--	4.2	--	3.4	0.12		
97.5%	--	78.7	--	9.9	--	34.3	0.25		
Decollement segment 3									
Lower	24	0	15	0	223	-90	0	26.9	65.1
Upper	same	100	same	10	same	90	8.0		
Optimal	--	42.9	--	5.6	--	-2.9	0.19		
2.5%	--	16.8	--	2.5	--	-34.6	0.09		
97.5%	--	66.6	--	8.9	--	25.1	0.30		
Decollement segment 4									
Lower	24	0	15	0	230	-90	0	26.8	65.0
Upper	same	100	same	10	same	90	8.0		
Optimal	--	58.2	--	2.7	--	38.9	0.25		
2.5%	--	46.1	--	0.0	--	21.6	0.18		
97.5%	--	71.7	--	6.5	--	55.1	0.33		
Decollement segment 5									
Lower	32	0	15	0	238	-90	0	26.6	64.9
Upper	same	100	same	10	same	90	8.0		
Optimal	--	52.4	--	7.4	--	28.1	0.33		
2.5%	--	43.6	--	3.1	--	19.1	0.26		
97.5%	--	61.1	--	9.9	--	37.1	0.40		
Decollement segment 6									
Lower	32	0	15	0	242	-90	0	26.4	64.6
Upper	same	100	same	10	same	90	8.0		
Optimal	--	45.6	--	7.3	--	16.6	0.26		
2.5%	--	32.3	--	1.4	--	4.1	0.18		
97.5%	--	61.4	--	9.9	--	28.8	0.34		
Decollement segment 7									
Lower	40	0	15	0	251	-90	0	26.2	64.4
Upper	same	100	same	10	same	90	8.0		
Optimal	--	5.2	--	5.6	--	43.8	0.28		

2.5%	--	1.00	--	1.6	--	24.6	0.01
97.5%	--	16.2	--	9.7	--	55.8	0.62

Table S2.4. Same as Table S2.1 but for mid-prism decollement model of time period 1.

	Length (km)	Width (km)	Depth (km)	Dip (°)	Strike (°)	Rake (°)	Net slip (m)	lat	lon	Mw	Rms (m)
Coseismic segment 1											
Lower	48	0	0	60	203	-90	0			7.05	0.012
Upper	same	70	20	Same as above		90	1.5				
Optimal	--	36.4	6.81	--	--	13.50	0.19	27.16	65.45		
2.5%	--	24.5	2.3	--	--	-7.00	0.05				
97.5%	--	50.1	13.55	--	--	35.32	0.39				
Coseismic segment 2											
Lower	32	0	0	70	216	-90	0				
Upper	same	70	20	Same as above		90	1.5				
Optimal	--	49.5	12.49	--	--	52.84	0.11	27.37	65.67		
2.5%	--	26.9	6.29	--	--	19.63	0.06				
97.5%	--	69.7	18.67	--	--	82.93	0.18				
Coseismic segment 3											
Lower	24	0	0	47	223	-90	0				
Upper	same	70	20	Same as above		90	1.5				
Optimal	--	28.2	11.69	--	--	17.10	0.15	26.80	65.25		
2.5%	--	13.2	4.73	--	--	-7.8	0.00				
97.5%	--	45.4	17.91	--	--	42.34	0.41				
Coseismic segment 4											
Lower	24	0	0	47	230	-90	0				
Upper	same	70	20	Same as above		90	1.5				
Optimal	--	47.8	13.19	--	--	44.67	0.14	26.67	65.10		
2.5%	--	14.3	7.68	--	--	17.91	0.06				
97.5%	--	69.9	19.99	--	--	69.84	0.22				
Coseismic segment 5											
Lower	32	0	0	56	238	-90	0				
Upper	same	70	20	Same as above		90	1.5				
Optimal	--	46.9	12.51	--	--	27.84	0.15	26.52	64.94		
2.5%	--	20.9	6.75	--	--	11.16	0.08				
97.5%	--	68.2	17.73	--	--	48.25	0.22				
Coseismic segment 6											
Lower	32	0	0	56	242	-90	0				
Upper	same	70	20	Same as above		90	1.5				
Optimal	--	19.7	11.91	--	--	28.53	0.16	26.37	64.68		
2.5%	--	2.8	6.51	--	--	-4.41	0.02				
97.5%	--	42.1	16.85	--	--	61.10	0.38				
Coseismic segment 7											
Lower	40	0	0	56	251	-90	0				
Upper	same	70	20	Same as above		90	1.5	26.24	64.42		

Optimal	--	9.6	10.66	--	--	1.82	0.16	
2.5%	--	0.02	6.86	--	--	-12.3	0.00	
97.5%	--	25.7	13.93	--	--	22.42	0.42	

Table S3.1. Same as Table S2.1 but for time period 2

	Length (km)	Width (km)	Depth (km)	Dip (°)	Strike (°)	Rake (°)	Net slip (m)	lat	lon	Mw	Rms (m)
Coseismic segment 1											
Lower	48	30.0	0	60	203	-90	0			7.10	0.011
Upper		Same as above				90	5.0				
Optimal	--	--	--	--	--	-5.3	0.03	27.1	65.5		
2.5%	--	--	--	--	--	-29.5	0.01				
97.5%	--	--	--	--	--	27.9	0.05				
Coseismic segment 2											
Lower	32	27.7	0	70	216	-90	0				
Upper		Same as above				90	5.0				
Optimal	--	--	--	--	--	-10.0	0.01	27.3	65.7		
2.5%	--	--	--	--	--	-29.9	0.00				
97.5%	--	--	--	--	--	11.0	0.03				
Coseismic segment 3											
Lower	24	35.6	0	47	223	-90	0				
Upper		Same as above				90	5.0				
Optimal	--	--	--	--	--	41.3	0.02	26.7	65.3		
2.5%	--	--	--	--	--	14.5	0.00				
97.5%	--	--	--	--	--	67.3	0.04				
Coseismic segment 4											
Lower	24	35.6	0	47	230	-90	0				
Upper		Same as above				90	5.0				
Optimal	--	--	--	--	--	51.8	0.02	26.6	65.2		
2.5%	--	--	--	--	--	14.5	0.00				
97.5%	--	--	--	--	--	86.0	0.03				
Coseismic segment 5											
Lower	32	31.4	0	56	238	-90	0				
Upper		Same as above				90	5.0				
Optimal	--	--	--	--	--	22.2	0.004	26.5	64.9		
2.5%	--	--	--	--	--	-14.9	0.00				
97.5%	--	--	--	--	--	53.5	0.01				
Coseismic segment 6											
Lower	32	31.4	0	56	242	-90	0				
Upper		Same as above				90	5.0				
Optimal	--	--	--	--	--	45.1	0.008	26.3	64.7		
2.5%	--	--	--	--	--	13.8	0.0				
97.5%	--	--	--	--	--	75.8	0.02				
Coseismic segment 7											
Lower	40	31.4	0	56	251	-90	0				
Upper		Same as above				90	5.0				
Optimal	--	--	--	--	--	22.6	0.01	26.2	64.4		
2.5%	--	--	--	--	--	-20.2	0.0				
97.5%	--	--	--	--	--	61.1	0.02				
Decollement segment 1											
Lower	48	0	26	0	203	-90	0			27.2	65.4
Upper	same	70	same	10	same	90	8.0				

Optimal	--	55.9	--	7.9	--	24.9	0.16		
2.5%	--	46.6	--	2.9	--	12.3	0.12		
97.5%	--	65.7	--	9.9	--	39.3	0.21		
Decollement segment 2									
Lower	32	0	26	0	216	-90	0		
Upper	same	70	same	10	same	90	8.0		
Optimal	--	56.5	--	8.4	--	30.4	0.16	27.4	65.6
2.5%	--	46.3	--	3.9	--	9.0	0.10		
97.5%	--	66.9	--	9.6	--	50.3	0.22		
Decollement segment 3									
Lower	24	0	26	0	223	-90	0		
Upper	same	70	same	10	same	90	8.0		
Optimal	--	1.3	--	5.0	--	19.8	4.07	26.9	65.1
2.5%	--	0.1	--	0.2	--	-21.3	0.78		
97.5%	--	3.6	--	9.3	--	57.5	7.98		
Decollement segment 4									
Lower	24	0	26	0	230	-90	0		
Upper	same	70	same	10	same	90	8.0		
Optimal	--	7.1	--	4.5	--	20.4	0.92	26.8	65.0
2.5%	--	1.7	--	0.0	--	-9.7	0.26		
97.5%	--	15.3	--	9.2	--	46.9	2.12		
Decollement segment 5									
Lower	32	0	26	0	238	-90	0		
Upper	same	70	same	10	same	90	8.0		
Optimal	--	5.7	--	6.9	--	41.4	0.87	26.6	64.9
2.5%	--	1.1	--	3.8	--	17.1	0.19		
97.5%	--	10.7	--	9.9	--	66.7	2.41		
Decollement segment 6									
Lower	32	0	26	0	242	-90	0		
Upper	same	70	same	10	same	90	8.0		
Optimal	--	7.1	--	4.5	--	54.5	0.26	26.4	64.6
2.5%	--	0.0	--	0.1	--	21.6	0.10		
97.5%	--	19.7	--	9.1	--	87.7	0.38		
Decollement segment 7									
Lower	40	0	26	0	251	-90	0		
Upper	same	70	same	10	same	90	8.0		
Optimal	--	1.5	--	5.7	--	79.2	2.65	26.2	64.4
2.5%	--	0.4	--	0.4	--	58.2	0.58		
97.5%	--	3.9	--	9.7	--	89.9	5.23		

Table S3.2. Same as Table S2.3 but for time period 2.

	Length (km)	Width (km)	Depth (km)	Dip (°)	Strike (°)	Rake (°)	Net slip (m)	lat	lon	Mw	Rms (m)
Coseismic segment 1											
Lower	48	30.0	0	60	203	-90	0			7.1	0.010
Upper		Same as above				90	5.0				
Optimal	--	--	--	--	--	1.25	0.02	27.1	65.5		
2.5%	--	--	--	--	--	-29.3	0				
97.5%	--	--	--	--	--	29.7	0.05				
Coseismic segment 2											
Lower	32	27.7	0	70	216	-90	0			27.3	65.7
Upper		Same as above				90	5.0				

Optimal	--	--	--	--	--	19.8	0.01		
2.5%	--	--	--	--	--	-8.9	0.00		
97.5%	--	--	--	--	--	49.9	0.03		
Coseismic segment 3									
Lower	24	35.6	0	47	223	-90	0		
Upper		Same as above				90	5.0		
Optimal	--	--	--	--	--	46.9	0.02	26.7	65.3
2.5%	--	--	--	--	--	22.0	0.00		
97.5%	--	--	--	--	--	66.9	0.04		
Coseismic segment 4									
Lower	24	35.6	0	47	230	-90	0		
Upper		Same as above				90	5.0		
Optimal	--	--	--	--	--	38.6	0.01	26.6	65.2
2.5%	--	--	--	--	--	10.0	0.00		
97.5%	--	--	--	--	--	70.1	0.03		
Coseismic segment 5									
Lower	32	31.4	0	56	238	-90	0		
Upper		Same as above				90	5.0		
Optimal	--	--	--	--	--	-13.9	0.004	26.5	64.9
2.5%	--	--	--	--	--	-39.9	0.00		
97.5%	--	--	--	--	--	20.3	0.01		
Coseismic segment 6									
Lower	32	31.4	0	56	242	-90	0		
Upper		Same as above				90	5.0		
Optimal	--	--	--	--	--	23.3	0.005	26.3	64.7
2.5%	--	--	--	--	--	5.9	0.0		
97.5%	--	--	--	--	--	45.9	0.01		
Decollement segment 1									
Lower	48	0	15	0	203	-90	0		
Upper	same	100	same	10	same	90	8.0		
Optimal	--	84.6	--	7.7	--	22.5	0.12	27.2	65.4
2.5%	--	67.9	--	2.6	--	13.4	0.08		
97.5%	--	99.7	--	9.9	--	31.9	0.16		
Decollement segment 2									
Lower	32	0	15	0	216	-90	0		
Upper	same	100	same	10	same	90	8.0		
Optimal	--	76.4	--	7.6	--	31.8	0.10	27.4	65.6
2.5%	--	43.6	--	1.7	--	10.3	0.05		
97.5%	--	99.9	--	9.9	--	6.9	0.14		
Decollement segment 3									
Lower	24	0	15	0	223	-90	0		
Upper	same	100	same	10	same	90	8.0		
Optimal	--	7.9	--	4.4	--	19.8	0.44	26.9	65.1
2.5%	--	1.4	--	0	--	-7.4	0.05		
97.5%	--	25.2	--	9.8	--	50.3	1.10		
Decollement segment 4									
Lower	24	0	15	0	230	-90	0	26.8	65.0

Upper	same	100	same	10	same	90	8.0	
Optimal	--	47.0	--	7.3	--	46.2	0.16	
2.5%	--	33.5	--	1.7	--	31.2	0.10	
97.5%	--	63.3	--	9.9	--	60.0	0.22	
Decollement segment 5								
Lower	32	0	15	0	238	-90	0	
Upper	same	100	same	10	same	90	8.0	
Optimal	--	53.1	--	6.6	--	40.8	0.15	26.6 64.9
2.5%	--	28.9	--	0.8	--	25.7	0.09	
97.5%	--	77.4	--	9.9	--	56.4	0.20	
Decollement segment 6								
Lower	32	0	15	0	242	-90	0	
Upper	same	100	same	10	same	90	8.0	
Optimal	--	44.5	--	5.9	--	44.1	0.11	26.4 64.6
2.5%	--	20.9	--	0.3	--	25.4	0.05	
97.5%	--	82.4	--	9.9	--	63.9	0.16	
Decollement segment 7								
Lower	40	0	15	0	251	-90	0	
Upper	same	100	same	10	same	90	8.0	
Optimal	--	14.9	--	6.9	--	60.5	0.15	26.2 64.4
2.5%	--	3.0	--	1.8	--	36.5	0.05	
97.5%	--	38.1	--	9.9	--	88.5	0.31	

Table S3.3. Same as Table S2.4 but for time period 2.

		Seg1	Seg2	Seg3	Seg4	Seg5	Seg6	Seg7	Average
Basal decollement model									
Tp1	Maximum ss	32.33	20.96	11.66	9.89	5.43	-3.70	3.64	11.46
	Aseismic slip	28.95	10.42	-67.16	53.70	24.46	33.30	51.93	19.37
Tp2	Maximum ss	35.25	26.39	-1.57	-1.39	4.32	-5.15	2.48	8.62
	Aseismic slip	30.39	24.92	19.81	20.44	41.44	54.49	79.16	38.66
Mid-prism decollement model									
Tp1	Maximum ss	17.85	29.84	20.25	-7.60	-4.83	16.94	-16.53	7.99
	Aseismic slip	19.12	13.35	-2.932	38.86	28.15	16.60	43.82	22.42
Tp2	Maximum ss	25.65	31.53	-7.57	-10.74	-4.89	18.21	58.20	15.77
	Aseismic slip	31.82	22.46	19.81	46.22	40.88	44.05	60.48	37.96

Table S4. Direction (rake angle) of maximum coseismic shear stress and aseismic slip of basal decollement model and mid-prism decollement model. 'Maximum ss' means maximum coseismic shear stress.